Robert SURUS, Tomasz TARCZEWSKI

Nicolaus Copernicus University in Torun, Insitute of Engineering and Technology

Finite Control Set Model Predictive Current Control for Reluctance Synchronous Motor - Current Ripple Analysis

Abstract. *The paper presents a finite control set model predictive current control FCS-MPC for reluctance synchronous motor (RSM). A detailed mathematical description of the maximum range of current ripple amplitude is presented, taking into account the most accurate model of a synchronous reluctance motor containing four inductance components. The experimental studies carried out indicate the correct analytical mathematical model to determine the amplitude of current ripples, both for low and high switching frequencies of the SiC MOSFET's.*

Streszczenie. *W artykule przedstawiono sterowanie predykcyjne prądami synchronicznego silnika reluktancyjnego. Przedstawiono szczegółowy opis matematyczny pozwalający na wyliczenie maksymalnego zakresu tętnień prądu, z uwzględnieniem najdokładniejszego modelu synchronicznego silnika reluktancyjnego zawierającego cztery składowe indukcyjności. Przeprowadzone badania eksperymentalne wskazują na poprawny analityczny model matematyczny w celu wyznaczenia amplitudy tętnień prądu, zarówno dla niskich jak i wysokich częstotliwości kluczowania tranzystorów przekształtnika. (Sterowanie predykcyjne prądu dla synchronicznego silnika reluktancyjnego - analiza tętnień prądu)*

Keywords: Finite Control Set, Model Predictive Current Control, Reluctance Synchronous Motor, Current Ripples
Słowa kluczowe: Skończony Zbiór Sterowania, Sterowanie Predykcyjne Prądami, Synchroniczny Silnik Reluktancyjny, Tętnienia Prądu

Introduction

Reluctance synchronous motors (RSM) exhibit notable energy efficiency and torque, even in the absence of permanent magnets [1, 2]. A crucial role in electromobility and the reduction of carbon dioxide emissions are the main reasons, why RSMs are used [3]. The design of the rotor contributes to variable inductance on the motor windings which is dependent upon the current flow [4]. For precise torque and speed control, an accurate mathematical model is required. The stator construction of RSM, Permanent Magnet Synchronous Motor (PMSM), and Induction Motor (IM) is analogous, enabling the utilization of a cascade control structure with a field-oriented control strategy [5]. A limited bandwidth resulting modest speed control dynamic is the main disadvantage of this solution. Instead of the conventional cascade control structure (CCS), the state feedback controller (SFC) [1, 6, 7], the sliding mode controller [8, 9], adaptive controllers [10], and model predictive control (MPC) [11, 12, 13] can be employed. Model predictive control is characterized by superior dynamical behavior, lack of tuning procedure, and intuitive concept. This strategy seems to be a promising approach for RSM and a good alternative for other control structures such as CCS or SFC [1, 6, 7]. Differentiating among various types of MPC, two main categories can be identified: finite control set MPC (FCS-MPC) and continuous set MPC (CS-MPC) [12, 13, 14]. Various approaches to implementing the FCS-MPC structure have been taken for the induction motor [15]. Throughout the optimization process, the designated cost function is minimized, leading to the acquisition of an optimal voltage vector. The analyzed control configuration functions without a space vector modulation (SVM) and exhibits a reduced set of parameters in comparison to the field-oriented control structure. For RSM, a solution is not suitable, because it may result in electrical time constant mismatch and poor current control performances [16].

To contribute to increasing the service life of the motor's mechanical components, it is important to minimize the impact of current and torque ripples. The inverters used in industry are built of transistors that have a low switching frequency. Nowadays, inverters with SiC-MOSFET's modules [17, 18], which are characterized by a high switching frequency can be applied to reduce the switching period and, as a result, to mitigate the phase currents ripple. Since the above-mentioned ripple directly impacts the control performance, it is reasonable to rate its level during the synthesis of the control system. As shown in [19, 20], this task can be accomplished using the analysis of the peak-to-peak distribution of current ripples in the sampling period.

In this paper, the modeling and evaluation of current ripple amplitude in FCS-MPCC for RSM were presented. Numerical tests and experimental studies were carried out to confirm the correctness of the analytical modeling of the current ripple amplitude for two sampling frequencies of 10 kHz and 25 kHz.

Mathematical model of drive

The RSM control is realized in a rotating reference frame (RRF) coordinate system, which requires the mathematical model to be defined as D- and Q-axis components of flux linkage and current. The model of RSM can be represented by the following equations [14, 16]:

(1) $$\frac{d\psi_d(t)}{dt} = u_{sd}(t) - Ri_{sd}(t) + n_p\omega_m(t)\psi_q(t)$$

(2) $$\frac{d\psi_q(t)}{dt} = u_{sq}(t) - Ri_{sq}(t) - n_p\omega_m(t)\psi_d(t)$$

(3) $$J\frac{d\omega_m(t)}{dt} = \frac{3}{2}n_p(\psi_d(t)i_{sq}(t) - \psi_q(t)i_{sd}(t)) - \\ - B\omega_m(t) - T_L(t)$$

(4) $$\psi_d(t) = L_d\Big(i_{sd}(t), i_{sq}(t)\Big)i_{sd}(t)$$

(5) $$\psi_q(t) = L_q\Big(i_{sd}(t), i_{sq}(t)\Big)i_{sq}(t)$$

where: $u_d(t)$ and $u_q(t)$ - input voltages given in RRF, $i_{sd}(t)$ and $i_{sq}(t)$ - stator current components given in RRF, $\psi_d(t)$ and $\psi_q(t)$ - magnetic flux components, R - stator resistance, n_p - number of pole pairs, $\omega_m(t)$ - rotational velocity of the rotor, J - moment of inertia, B - viscous friction coefficient, and $T_L(t)$ - external load torque. Using identification by indirect measurement of magnetic fluxes associated with the components of the stator current, four components of the motor inductances can be determined. The polynomial approximation in the Matlab environment, for determining surfaces of inductances can be used [4]. Since the magnetic saturation phenomenon occurs, the D- and Q-axis components of the inductance are strongly non-linear and current dependent. The assumed characteristics of $L_{dd}(i_{sd}, i_{sq})$, $L_{dq}(i_{sd}, i_{sq})$,
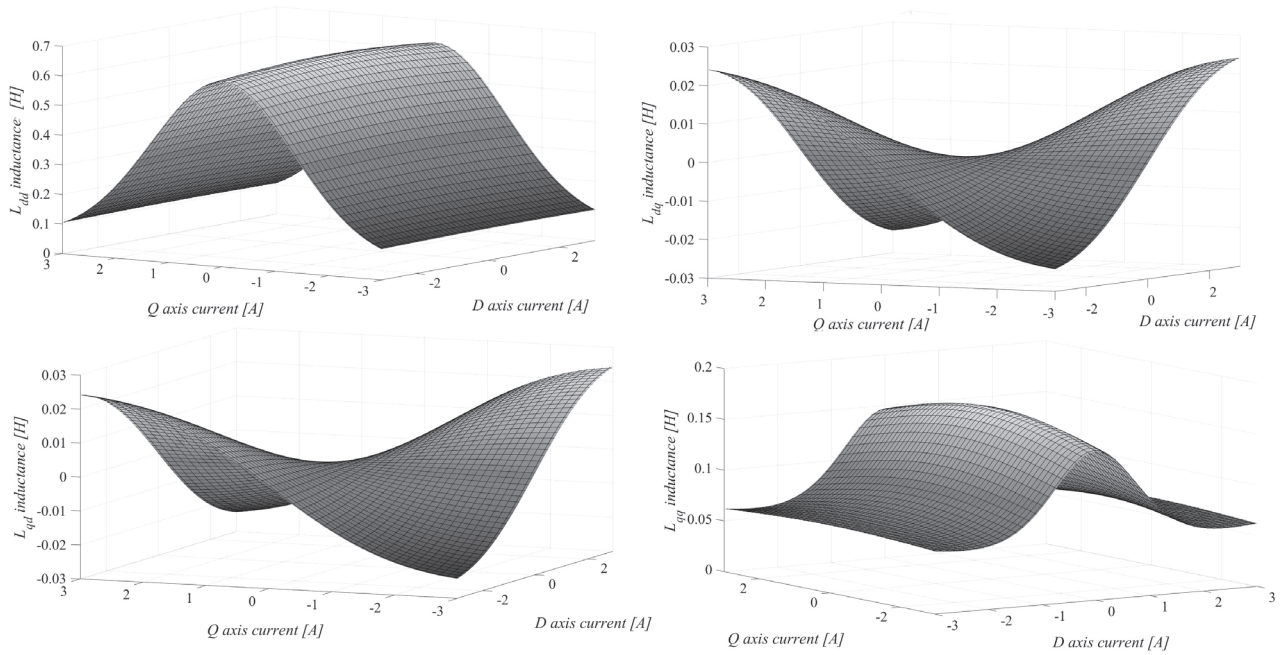
Fig. 1. The determined characteristics of L_{dd}, L_{dq}, L_{qd} and L_{qq} inductances

$L_{qd}(i_{sd}, i_{sq})$ and $L_{qq}(i_{sd}, i_{sq})$ are presented on Fig. 1. Using four inductance components makes it possible to obtain a more accurate mathematical RSM model than the model presented in [21]. The equations for L_{dd}, L_{dq}, L_{qd} and L_{qq} are written as [4, 16]:

(6)
$$L_{dd}(i_{sd}, i_{sq}) = A_0 - i_{sd}(L_{d0}(i_{sd}) + L_{d1}(i_{sd}, i_{sq})) + L_{d2}(i_{sd}) + L_{d3}(i_{sd}, i_{sq})$$

(7)
$$L_{dq}(i_{sd}, i_{sq}) = \frac{-2B_1 C_q i_{sd} i_{sq}}{(C_q i_{sq}^2 + 1)^2 (i_{sd}^4 + C_1 i_{sd}^2 + D_1)}$$

(8)
$$L_{qd}(i_{sd}, i_{sq}) = \frac{-2B_3 C_d i_{sd} i_{sq}}{(C_d i_{sd}^2 + 1)^2 (i_{sq}^4 + C_3 i_{sq}^2 + D_3)}$$

(9)
$$L_{qq}(i_{sd}, i_{sq}) = A_2 - i_{sq}(L_{q0}(i_{sq}) + L_{q1}(i_{sd}, i_{sq})) + L_{q2}(i_{sq}) + L_{q3}(i_{sd}, i_{sq})$$

where:

(10)
$$L_{d0}(i_{sd}) = \frac{B_0(4i_{sd}^3 + 2C_0 i_{sd})}{(i_{sd}^4 + C_0 i_{sd}^2 + D_0)^2}$$

(11)
$$L_{d1}(i_{sd}, i_{sq}) = \frac{B_1\left(\frac{1}{C_q i_{sq}^2 + 1}\right)\left(4i_{sd}^3 + 2C_1 i_{sd}^2 + i_{sd}^4\right)}{(i_{sd}^4 + C_1 i_{sd}^2 + D_1)^2}$$

(12)
$$L_{d2}(i_{sd}) = \frac{B_0}{(i_{sd}^4 + C_0 i_{sd}^2 + D_0)^2}$$

(13)
$$L_{d3}(i_{sd}, i_{sq}) = \frac{B_1\left(\frac{1}{C_q i_{sq}^2 + 1}\right)}{i_{sd}^4 + C_1 i_{sd}^2 + D_1}$$

(14)
$$L_{q0}(i_{sq}) = \frac{B_2(4i_{sq}^3 + 2C_2 i_{sq})}{(i_{sq}^4 + C_2 i_{sq}^2 + D_2)^2}$$

(15)
$$L_{q1}(i_{sd}, i_{sq}) = \frac{B_3\left(\frac{1}{C_d i_{sd}^2 + 1}\right)\left(4i_{sq}^3 + 2C_3 i_{sq}^2 + i_{sq}^4\right)}{(i_{sq}^4 + C_3 i_{sq}^2 + D_3)^2}$$

(16)
$$L_{q2}(i_{sq}) = \frac{B_2}{(i_{sq}^4 + C_2 i_{sq}^2 + D_2)^2}$$

(17)
$$L_{q3}(i_{sd}, i_{sq}) = \frac{B_3\left(\frac{1}{C_d i_{sd}^2 + 1}\right)}{i_{sq}^4 + C_3 i_{sq}^2 + D_3}$$

where: A_0, B_0, C_0, D_0, A_1, B_1, C_1, D_1 and C_q are the constant coefficients in $L_{dd}(i_{sd}, i_{sq})$ and $L_{dq}(i_{sd}, i_{sq})$, while A_2, B_2, C_2, D_2, A_3, B_3, C_3, D_3 and C_d are the constant coefficients in $L_{qd}(i_{sd}, i_{sq})$ and $L_{qq}(i_{sd}, i_{sq})$.

Values of the inductance coefficients were determined by indirect measurement of the magnetic flux for different values of the current components and the polynomial approximation. These are presented in Table 1. From obtained re-

Table 1. Values of constants for the approximation of inductance

A_0	B_0	C_0	D_0
0.184	134.32	34.7	290.22

B_1	C_1	D_1	C_q
1379	684.2	10237	0.024

A_2	B_2	C_2	D_2
0.078	17353	57359	19001

B_3	C_3	D_3	C_d
265.17	119.41	2411.8	0.029

sults, one can see that there is a relatively high difference between the lower and the higher value of the inductance what resulting a direct impact on the current ripple from power converter switching. On the other hand, the switching period should also be taken into account, especially if modern power converter stage is utilized allowing relatively short switching period and acceptable switching losses. Respective analysis for RSM with FCS-MPC will be conducted in the remainder part of this paper.
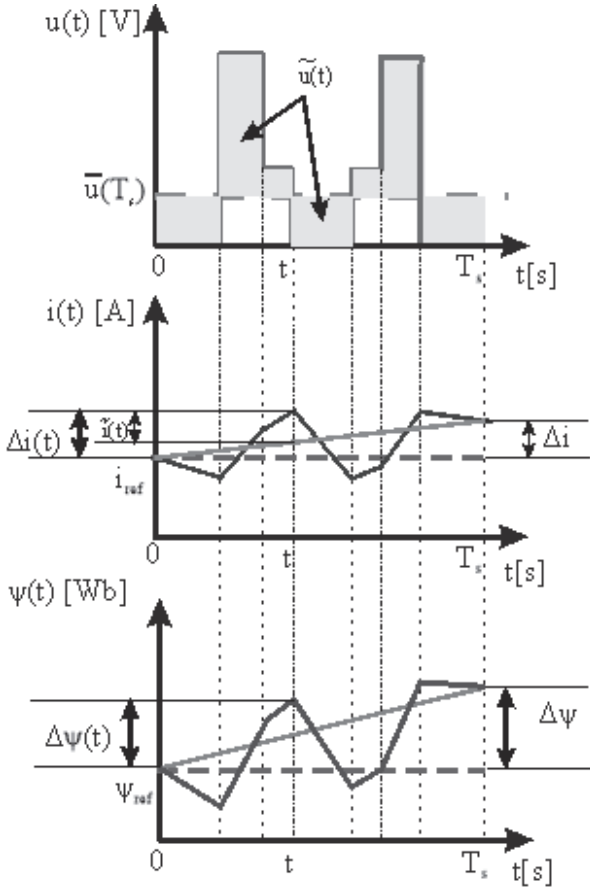
Fig. 2. Details of generic output voltage, current and flux in the one switching period

Mathematical analysis of current ripple

Conducting the analysis of current ripple requires the voltage equation describing RSM fed from VSI. This is as follows

(18) $$\begin{bmatrix} u_{sd}(t) \\ u_{sq}(t) \end{bmatrix} = R \begin{bmatrix} i_{sd}(t) \\ i_{sq}(t) \end{bmatrix} + \frac{d}{dt} \begin{bmatrix} \psi_d(t) \\ \psi_q(t) \end{bmatrix} + \begin{bmatrix} v_{gd}(t) \\ v_{gq}(t) \end{bmatrix}$$

where $v_{gd}(t)$ and $v_{gq}(t)$ are the electromotive force (EMF) in RRF. Equation (18) can be averaged over the switching period T_s leading to

(19) $$\begin{bmatrix} \bar{u}_{sd}(T_s) \\ \bar{u}_{sq}(T_s) \end{bmatrix} = R \begin{bmatrix} \bar{i}_{sd}(T_s) \\ \bar{i}_{sq}(T_s) \end{bmatrix} + \frac{1}{T_s} \begin{bmatrix} \Delta\psi_d \\ \Delta\psi_q \end{bmatrix} + \begin{bmatrix} \bar{v}_{gd}(T_s) \\ \bar{v}_{gq}(T_s) \end{bmatrix}$$

with

(20) $$\Delta\psi_d = \psi_d(T_s) - \psi_d(0)$$

(21) $$\Delta\psi_q = \psi_q(T_s) - \psi_q(0)$$

The alternating components of voltages can be written by introducing the average over switching period as

(22) $$\begin{bmatrix} \tilde{u}_{sd}(t) \\ \tilde{u}_{sq}(t) \end{bmatrix} = \begin{bmatrix} u_{sd}(t) \\ u_{sq}(t) \end{bmatrix} - \begin{bmatrix} \bar{u}_{sd}(T_s) \\ \bar{u}_{sq}(T_s) \end{bmatrix}$$

By introducing (18) and (19) in (22) leads to:

(23) $$\begin{bmatrix} \tilde{u}_{sd}(t) \\ \tilde{u}_{sq}(t) \end{bmatrix} = R \begin{bmatrix} i_{sd}(t) - \bar{i}_{sd}(T_s) \\ i_{sq}(t) - \bar{i}_{sd}(T_s) \end{bmatrix} +$$
$$\begin{bmatrix} \frac{d}{dt}\psi_d(t) - \frac{\Delta\psi_d}{T_s} \\ \frac{d}{dt}\psi_q(t) - \frac{\Delta\psi_q}{T_s} \end{bmatrix} + \begin{bmatrix} v_{gd}(t) - \bar{v}_{gd}(T_s) \\ v_{gq}(t) - \bar{v}_{gq}(T_s) \end{bmatrix}$$

The first and the third term in (23) can be neglected [19] leading to

(24) $$\begin{bmatrix} \tilde{u}_{sd}(t) \\ \tilde{u}_{sq}(t) \end{bmatrix} = \begin{bmatrix} \frac{d}{dt}\psi_d(t) - \frac{\Delta\psi_d}{T_s} \\ \frac{d}{dt}\psi_q(t) - \frac{\Delta\psi_q}{T_s} \end{bmatrix}$$

The flux and current variation in sub-period [0, t] are depicted in Fig. 2 and can be calculated from (24) as

(25) $$\begin{bmatrix} \Delta\psi_d(t) \\ \Delta\psi_q(t) \end{bmatrix} = \int_0^t \begin{bmatrix} \tilde{u}_{sd}(t) \\ \tilde{u}_{sq}(t) \end{bmatrix} dt + \frac{t}{T_s} \begin{bmatrix} \Delta\psi_d \\ \Delta\psi_q \end{bmatrix}$$

(26) $$\begin{bmatrix} \Delta i_{sd}(t) \\ \Delta i_{sq}(t) \end{bmatrix} = L^{-1} \left(\int_0^t \begin{bmatrix} \tilde{u}_{sd}(t) \\ \tilde{u}_{sq}(t) \end{bmatrix} dt + \frac{t}{T_s} \begin{bmatrix} \Delta\psi_d \\ \Delta\psi_q \end{bmatrix} \right)$$

where:

(27) $$L = \begin{bmatrix} L_{dd} & L_{dq} \\ L_{qd} & L_{qq} \end{bmatrix}$$

Equation (26) allows to define the instantaneous current ripple as

(28) $$\begin{bmatrix} \tilde{i}_{sd}(t) \\ \tilde{i}_{sq}(t) \end{bmatrix} = L^{-1} \int_0^t \begin{bmatrix} \tilde{u}_{sd}(t) \\ \tilde{u}_{sq}(t) \end{bmatrix} dt$$

The peak-to-peak current ripple can be defined as

(29) $$\begin{bmatrix} \tilde{i}_{ppd} \\ \tilde{i}_{ppq} \end{bmatrix} = \max \begin{bmatrix} \tilde{i}_{sd}(T_s) \\ \tilde{i}_{sq}(T_s) \end{bmatrix} - \min \begin{bmatrix} \tilde{i}_{sd}(T_s) \\ \tilde{i}_{sq}(T_s) \end{bmatrix}$$

In order to estimate current ripple amplitude in the whole fundamental period, the maximum and the minimum values of the current must be evaluated. The simplified expression for maximum of peak-to-peak current ripple amplitude, for modulation index larger than 0.282 [19] can be written as

(30) $$\max \begin{bmatrix} \tilde{i}_{ppdd} & \tilde{i}_{ppdq} \\ \tilde{i}_{ppqd} & \tilde{i}_{ppqq} \end{bmatrix} = \begin{bmatrix} L^{-1} \end{bmatrix} \frac{V_{dc} T_s m}{2\sqrt{3}}$$

(31) $$\tilde{i}_{ppd} = \tilde{i}_{ppdd} + \tilde{i}_{ppdq}$$

(32) $$\tilde{i}_{ppq} = \tilde{i}_{ppqd} + \tilde{i}_{ppqq}$$

where m is a is a modulation index and equal to $\frac{\sqrt{3}}{3}$ for numerical and experiment tests.

Control structure

The proposed control structure is based on a cascade connection of the angular velocity controller and model predictive current control (MPCC) structures. As shown in Fig. 3, the MTPA strategy has been applied to improve the efficiency of the RSM [14, 22]. The output signal of the velocity controller sets the demand torque for the MTPA block. For the angular velocity regulation, a PI controller was employed with coefficients selected using the Ziegler-Nichols second criterion [15, 20]. The overall block diagram of the control structure is presented in Fig. 3. To formulate the FCS-MPCC sheme, it is necessary to establish a suitable cost function and a corresponding discrete forecast model for the RSM electrical component. In this approach, the following cost
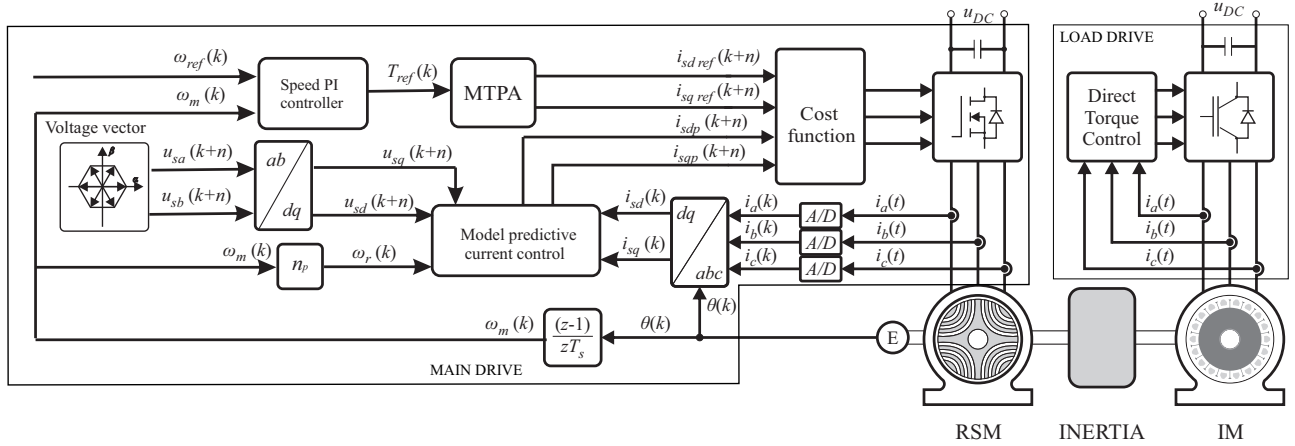
Fig. 3. Block diagram of the PI-MTPA-MPCC control structure for Reluctance synchronous motor

function was adopted:

(33)
$$g = \sum_{n=1}^{N} \Big(\big(i_{sdref}(k+n) - i_{sdp}(k+n) \big)^2 +$$
$$+ \big(i_{sqref}(k+n) - i_{sqp}(k+n) \big)^2 \Big)$$

where: g - the cost function, $i_{sdref}(k+n)$ and $i_{sqref}(k+n)$ - reference rotor and stator current components in next moment of time, $i_{sdp}(k+n)$ and $i_{sqp}(k+n)$ - predictive rotor and stator current components in next moment of time, N - the prediction horizon. Values of the cost function are subject to the minimization process. For the minimized cost function, appropriate voltage vectors were determined. An Euler discretization was applied to formulas (1)–(5) to obtain the discrete current-prediction model. As in input, eight different voltage vectors are used in each prediction step [11, 16, 21]. Then, Park transformation is provided to convert the voltages into RRF. The dependence between the prediction horizon and the number of possible cost functions is an exponential one. For a conventional FCS-MPCC we get the following relationship:

(34)
$$m = 7^N$$

where m is the number of possible cost function values and N is the prediction horizon.

In the most accurate MPCC approach, all components of the motor inductances (i.e., L_{dd}, L_{dq}, L_{qd}, L_{qq}) dependent on the currents i_{sd}, i_{sq} are considered.

The discrete formulas that describe predictive currents of RSM take the following form:

(35)
$$i_{sdp}(k+1) = \frac{\alpha_0(k)i_{sd}(k) + \alpha_1(k) + \alpha_2(k) + \alpha_3(k)}{\alpha_0(k)}$$

(36)
$$i_{sqp}(k+1) = \frac{-\alpha_0(k)i_{sq}(k) + \alpha_4(k) + \alpha_5(k) + \alpha_6(k)}{\alpha_0(k)}$$

where:

(37)
$$\alpha_0(k) = L_{dd}\Big(i_{sd}(k), i_{sq}(k)\Big) L_{qq}\Big(i_{sd}(k), i_{sq}(k)\Big) +$$
$$-L_{dq}\Big(i_{sd}(k), i_{sq}(k)\Big) L_{qd}\Big(i_{sd}(k), i_{sq}(k)\Big)$$

(38) $\alpha_1(k) = L_{qq}\Big(i_{sd}(k), i_{sq}(k)\Big) T_s \Big(u_{sd}(k) - Ri_{sd}(k)\Big)$

(39) $\alpha_2(k) = L_{dq}\Big(i_{sd}(k), i_{sq}(k)\Big) T_s \Big(Ri_{sq}(k) - u_{sq}(k)\Big)$

(40)
$$\alpha_3(k) = L_{dd}\Big(i_{sd}(k), i_{sq}(k)\Big) T_s n_p \omega(k) \Big(L_{qq}\Big(i_{sd}(k), i_{sq}(k)\Big)$$
$$+ i_{sq}(k) + L_{dq}\Big(i_{sd}(k), i_{sq}(k)\Big) i_{sd}(k)\Big)$$

(41) $\alpha_4(k) = L_{dd}\Big(i_{sd}(k), i_{sq}(k)\Big) T_s \Big(Ri_{sq}(k) - u_{sq}(k)\Big)$

(42)
$$\alpha_5(k) = -L_{qd}\Big(i_{sd}(k), i_{sq}(k)\Big) T_s \Big(u_{sd}(k) + Ri_{sd}(k)\Big)$$

(43)
$$\alpha_6(k) = T_s n_p \omega(k) \Big(L_{dd}^2\Big(i_{sd}(k), i_{sq}(k)\Big) i_{sd}(k) +$$
$$L_{qq}\Big(i_{sd}(k), i_{sq}(k)\Big) L_{qd}\Big(i_{sd}(k), i_{sq}(k)\Big) i_{sq}(k)\Big)$$

where: T_s is a sampling period, $i_{sd}(k)$ and $i_{sq}(k)$ are measured RRF current components. From (35)-(43), one can see that an accurate RSM model is relatively complex and therefore it is expected that its demand on computational resources will be high.

Experimental results

The experimental test-bed is shown in Fig. 4. It consists of a reluctance synchronous motor (3GAL092513-ASB) manufactured by ABB with a control unit, load drive with induction motor (3GAA092214-ASE) manufactured by ABB, two clutches and additional moment of inertia. The RSM control unit is based on a SiC-MOSFET power module and a NXP MKV58F1M0VLL24 microcontroller [16, 21]. The main parameters of the laboratory setup are listed in Table 2.

It was decided to verify the proposed approach for MPCC in experimental tests using an own-developed prototype of a voltage source inverter (VSI). Due to the limited computational resources of the microcontroller, experimental studies were carried out for the prediction horizon equal to 1. Since the current ripples depends on the switching
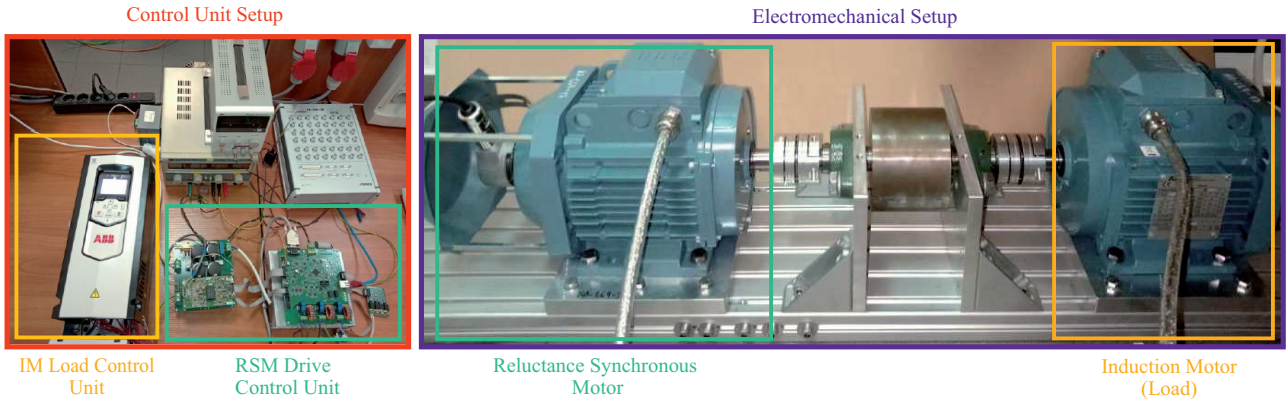
Fig. 4. Laboratory stand with RSM drive and IM load drive

Table 2. Parameters of reluctance synchronous motor drive

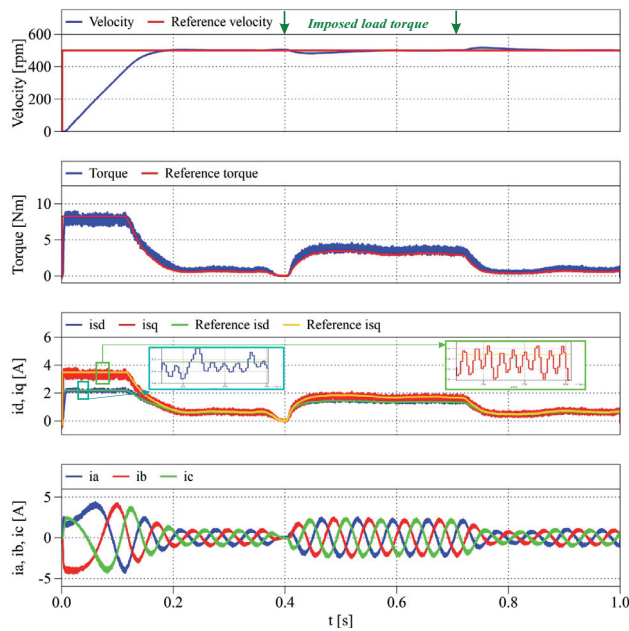| Parameter name	Symbol	Value	Unit
DC-link voltage	U_{DC}	450	V
Rated current (RMS)	I_N	2.9	A
Rated torque	T_N	7.0	Nm
Rated velocity	N_N	1500	rpm
Rated power	P_N	1.1	kW
Stator resistance	R	6.0	Ω
Number of pole pairs	n_p	2	-
Moment of inertia (summarized)	J	0.019	kgm^2
Viscous friction coefficient	B	0.015	Nms/rad

Fig. 5. Experimental results for velocity step response under load operation with proposed the MPCC strategy for the prediction horizon equal to 1 and sampling frequency 10 kHz

period (30), it was to decided to perform analysis for two switching frequencies: 10 kHz and 25 kHz. It is worth noting, that thanks to the modern power converter with efficient SiC-MOSFET modules, is possible to operate with relatively high switching frequencies. Finally, it should be noted that the delay compensation was implemented in analyzed control algorithm. The external load torque was imposed between $t \in [400; 700]$ ms. The dependence (30) uses a non-linear values of inductance as a function of currents. For the numerical determination of current ripples, the averaged values of
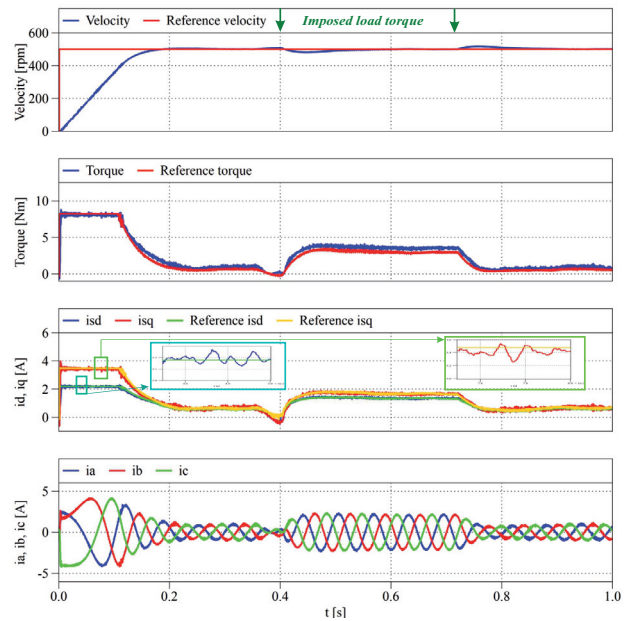

Fig. 6. Experimental results for velocity step response under load operation with proposed the MPCC strategy for the prediction horizon equal to 1 and sampling frequency 25 kHz

the inductance components, which were shown in Fig.1, were used. The obtained results were compared with experimental results, which are presented in Figs. 5 and 6. A reduction in the current and torque ripples with increasing switching frequency were observed. The waveform of the speed output signal confirms that the external load torque generated by the induction motor has been well-compensated. The values of current ripple from numerical and experimental tests are listed in Table 3.

Table 3. The values of current ripple from numerical and experimental tests for the averaged values of inductances

	Numerical results		Experimental tests	
f_s **[kHz]**	i_{ppd}**[A]**	i_{ppq}**[A]**	i_{ppd}**[A]**	i_{ppq}**[A]**
10	0.0503	0.1312	0.0498	0.1320
25	0.0198	0.0525	0.0200	0.0530

Conclusion

In this article, the output current ripple amplitude in Finite Control Set Model Predictive Current Control for Reluctance Synchronous Motor has been recognized and examined extensively. Simplified mathematical expressions to evaluate maximum current ripple are proposed and experimentally verified. The values of the current ripple obtained

from numerical tests are close to the values obtained on the experimental setup. The proposed formulas allow to precise calculation the current ripples to assure desired performance of the drive with FCS-MPC scheme. Future work will be focused on optimization model predictive control scheme for RSM in terms of computational complexity and current ripples.

REFERENCES

[1] T. Tarczewski, Ł. Niewiara, L.M. Grzesiak, "Artificial Neural Network-Based Gain-Scheduled State Feedback Speed Controller for Synchronous Reluctance Motor", *Power Electronics and Drives*, vol. 6, no. 1, pp.276–288, 2021

[2] H.A.A.Awan, S.E. Saarakkala, M. Hinkkanen, "Flux-Linkage-Based Current Control of Saturated Synchronous Motors," *IEEE Trans. Ind. Applicat.*, vol. 55, no. 5, pp. 4762–4769, 2019, doi: 10.1109/TIA.2019.2919258.

[3] Sustainable Transport, Electrifying the powertrains of industrial vehicles, transportation and marine - ABB white paper

[4] S. Yamamoto, K. Tomishige, T. Ara, "A method to calculate transient characteristics of synchronous reluctance motors considering iron loss and cross-magnetic saturation," in *Proc. 14th IAS Annual Meeting Conf. IA Conf.*, Hong Kong, China, 2005, pp. 1754–1761 Vol. 3, doi: 10.1109/IAS.2005.1518684.

[5] A.Niedworok, Ł. Orzech, "Assessment of efficiency of drive equipped with induction motor and drive equipped with reluctance motor", *Przeglad Elektrotechniczny*, R. 92 NR 8/2016 (in Polish)

[6] I. Boldea, L. Tutelea, "Reluctance Electric Machines: Design and Control", CRC Press, 2018

[7] T. Tarczewski, L.J. Niewiara, L.M. Grzesiak, "Gain-Scheduled State Feedback Speed Control of Synchronous Reluctance Motor," in *Proc. IEEE 19th Int. PEMC Conf.*, Gliwice, Poland, 2021, pp. 559–565, doi: 10.1109/PEMC48073.2021.9432549.

[8] N.Manuel, N. İnanç, "Sliding Mode Control-Based MPPT and Output Voltage Regulation of a Stand-alone PV System", *Power Electronics and Drives*, vol. 7, no. 1, 2022, pp. 159–173.

[9] X.Zhang, L. Sun, K. Zhao, L. Sun, "Nonlinear Speed Control for PMSM System Using Sliding-Mode Control and Disturbance Compensation Techniques," *IEEE Trans. Pow. Electron.*, vol. 28, no. 3, pp. 1358–1365, 2013, doi: 10.1109/TPEL.2012.2206610.

[10] H.Wang, H. Zhang, "An Adaptive Control Strategy for a Low-Ripple Boost Converter in BLDC Motor Speed Control", *Power Electronics and Drives*, vol. 6, no. 1, 2021, pp.242–259.

[11] A.Farhan, M. Abdelrahem, A. Saleh , A. Shaltout, R. Kennel, "Simplified Sensorless Current Predictive Control of Synchronous Reluctance Motor Using Online Parameter Estimation", *Energies* 2020, 13, 492.

[12] F. Wang, X. Mei, J. Rodriguez, R. Kennel, "Model predictive control for electrical drive systems-an overview," *CES Trans. on Electrical Machines and Systems*, vol. 1, no. 3, pp. 219-230, 2017, doi: 10.23919/TEMS.2017.8086100.

[13] K.Wróbel, P. Serkies, K. Szabat, "Model Predictive Base Direct Speed Control of Induction Motor Drive—Continuous and Finite Set Approaches", *Energies* 2020, 13, 1193.

[14] R.Surus, Ł.J. Niewiara, T.Tarczewski, "A computationally efficient finite control set model predictive current control for reluctance synchronous motor", Przegląd Elektrotechniczny, 2023, Vol.99 Issue 5, p243-250.

[15] Y. Yamamoto, S. Morimoto, M. Sanada, Y. Inoue, "Torque Ripple Reduction Using Asymmetric Flux Barriers in Synchronous Reluctance Motor," in *Proc. Int. IPEC-Niigata 2018 -ECCE Asia Conf.*, Niigata, Japan, 2018, pp. 3197–3202, doi: 10.23919/IPEC.2018.8507655.

[16] R.Surus, M. Tejer, Ł.J. Niewiara, T. Tarczewski, "An Impact of Model Accuracy on Control Performance in Finite Control Set Model Predictive Current Control for Reluctance Synchronous Motor", 36th International Conference on Electrical Drives and Power Electronics (EDPE 2023), The High Tatras, Slovakia

[17] D. Peftitsis and J. Rabkowski, "Gate and Base Drivers for Silicon Carbide Power Transistors: An Overview," in IEEE Transactions on Power Electronics, vol. 31, no. 10, pp. 7194-7213, Oct. 2016, doi: 10.1109/TPEL.2015.2510425.

[18] T. Tarczewski, M. Skiwski, L. M. Grzesiak, M. Zieliński (3918) PMSM Servo-Drive Fed by SiC MOSFETs Based VSI. Power Electronics and Drives,3(1) 35-45.

[19] G. Grandi and J. Loncarski, "Evaluation of current ripple amplitude in three-phase PWM voltage source inverters," 2013 International Conference-Workshop Compatibility And Power Electronics, Ljubljana, Slovenia, 2013, pp. 156-161, doi: 10.1109/CPE.2013.6601146.

[20] G.Grandi and J. Loncarski, "Evaluation of current ripple amplitude in five-phase PWM voltage source inverters," Eurocon 2013, Zagreb, Croatia, 2013, pp. 1073-1080, doi: 10.1109/EUROCON.2013.6625114.

[21] R.Surus, L.J. Niewiara, T. Tarczewski, L.M. Grzesiak, "Finite control set model predictive current control for reluctance synchronous motor," in *Proc. IEEE 20th Int. PEMC Conf.*, Brasov, Romania, 2022, pp. 235–242, doi: 10.1109/PEMC51159.2022.9962908.

[22] H.Mahmoud, G. Bacco, M. Degano, N. Bianchi, C. Gerada, "Synchronous Reluctance Motor Iron Losses: Considering Machine Nonlinearity at MTPA, FW, and MTPV Operating Conditions," *IEEE Trans. Energy Convers*, vol. 33, no. 3, pp. 1402–1410, 2018, doi: 10.1109/TEC.2018.2811543.